Relative dispersion and turbulence in the Southwestern Atlantic Ocean from drifters data

Stefano Berti[1] and Francisco Alves dos Santos[2]

[1] Laboratoire de Mécanique de Lille, CNRS/FRE 3723, Université de Lille, F-59000 Lille, France (E-mail: `stefano.berti@polytech-lille.fr`)
[2] PROOCEANO Serviço Oceanogràfico, Rio de Janeiro, Brazil

Abstract. Lagrangian data can provide relevant information on the advection and diffusion properties of geophysical flows at different scales of motion. In this study, the dispersion properties of an ensemble of trajectories transported by a surface ocean flow are analyzed. The data come from a set of Lagrangian drifters released in the South Brazilian Bight, during several oceanographic campaigns. Adopting a dynamical systems approach, the attention is primarily focused on scale-dependent indicators, like the finite-scale Lyapunov exponent. The relevance of mechanisms like two-dimensional turbulence for the dispersion process is addressed. Some deviations from the classical turbulent dispersion scenario in two-dimensions are found, likely to be ascribed to the nonstationary and nonhomogeneous characteristics of the flow. Relatively small-scale features (of order 1-10 km) are also considered to play a role in determining the properties of relative dispersion as well as the shape of the kinetic energy spectrum.
Keywords: Turbulent transport, Lagrangian dispersion, Geophysical flows, Oceanic turbulence.

1   Introduction

Experimental campaigns involving Lagrangian drifters provide useful information to test model and theories of geophysical fluid dynamics, as well as to characterize the advection and diffusion properties of flows in applications. In an oceanographic context, for instance, predicting the spreading of a pollutant or the distribution of a biological population (e.g., phytoplankton or fish larvae) transported by surface currents represent both a challenging scientific task and a matter of general interest.

In the past years, an amount of Lagrangian data about the South Atlantic Ocean (SAO) was collected thanks to the First GARP Global Experiment drifters, released following the major shipping lines, and to the Southern Ocean Studies drifters, deployed in the Brazil-Malvinas Confluence. These data allowed estimates of eddy kinetic energy, integral time scales and diffusivities [1,2]. Despite the relatively uniform coverage, the boundary currents resulted poorly populated by buoys. Furthermore, the majority of previous

studies about drifters in the South Atlantic have concerned one-particle statistics only. While single-particle statistics give information on the advective transport associated to the largest and most energetic scales of motion, two (or more) particle statistics are needed to access information about the dominant physical mechanism acting at a certain scale of motion (chaotic advection, turbulence, diffusion). In a previous study [3], we considered both one and two-particle statistics to investigate the advective and diffusive properties of the surface currents explored by an ensemble of drifters released in proximity of the coast of Brazil during a project called MONDO (Monitoring by Ocean Drifters), for the environmental assessment on an oil drilling operation. The analysis of trajectory pair dispersion revealed some deviations, at scales smaller than approximately 10 km, from the behavior expected within a classical two-dimensional (2D) turbulence scenario. Interestingly, such deviations suggest that motions in this range of scales would be more energetic than predicted by 2D turbulence. However, due to limited statistics, the results were not conclusive, i.e. no clear scaling behavior of appropriate statistical indicators was detected below 10 km.

In this study we revisit the analysis of trajectory pair dispersion in the Southwestern Atlantic Ocean using a larger data set, corresponding to drifter trajectories coming from environmental assessment projects of oil drilling operations (including the first MONDO project) and Projeto AZUL [4], a pilot operational oceanography program in the region. The main goal of the present work is to attempt making a step forward in the understanding of relative dispersion at scales smaller than 10 km, and discuss the consistency of the data analysis with classical turbulence theory predictions. The paper is organized as follows. In Section 2 we recall the classical picture of turbulent dispersion and we introduce the statistical indicators of Lagrangian dispersion that we will consider. In Section 3 we provide a description of the data set. In Section 4 we report the results of our data analysis, and in Sec. 5 we compare it with that issued from numerical simulations of the Lagrangian dispersion process. Finally, in Section 6 we provide some concluding remarks.

2   Turbulence and relative dispersion

In the quasi-geostrophic (QG) approximation, valid for relative vorticities much smaller than the ambient vorticity due to the Earth's rotation, theoretical arguments would predict that, from the scale of the forcing at which eddies are efficiently generated by instability, e.g. the Rossby radius of deformation δ_R, both a down-scale enstrophy cascade and an up-scale energy cascade take place. The corresponding energy spectra are respectively given by $E(k) \sim k^{-3}$ (for $k > k_R$) and $E(k) \sim k^{-5/3}$ (for $k < k_R$) [5,6], where k is the horizontal wavenumber and $k_R = 2\pi/\delta_R$. In the ocean, possible deviations from this ideal double-cascade scenario may come, reasonably, from the nonhomogeneous and nonstationary characteristics of the velocity field, e.g. in the case of boundary currents, as well as from ageostrophic effects. At this regard, one presently debated issue is the role of submesoscale structures [7], velocity field features

of size $\sim (1-10)$ km, in determining the shape of the energy spectrum at intermediate scales between the Rossby deformation radius, in the ocean typically $\sim (10-50)$ km, and the dissipative scales (much smaller than 1 km). It is worth observing, here, that recent high-resolution 3D simulations of upper-ocean turbulence [8,9] have shown that the direct cascade energy spectrum flattens from k^{-3} to k^{-2} at submesoscales.

Let us now see how different transport mechanisms, like the turbulent phenomenology described above, manifest in a Lagrangian framework, particularly from a relative dispersion perspective. Relative dispersion is defined as the second order moment of the distance $R(t) = ||\mathbf{r}^{(1)}(t) - \mathbf{r}^{(2)}(t)||$, at time t, between two trajectories:

$$\langle R^2(t)\rangle = \langle ||\mathbf{r}^{(1)}(t) - \mathbf{r}^{(2)}(t)||^2\rangle, \tag{1}$$

where the average is over all the available trajectory pairs $(\mathbf{r}^{(1)}, \mathbf{r}^{(2)})$. At scales smaller than the forcing scale, $\delta < \delta_R$, the presence of a direct enstrophy cascade implies that the velocity field varies smoothly in space. This means that, for nonlinear fields, the particle pair separation typically evolves following an exponential law:

$$\langle R^2(t)\rangle \sim e^{2\lambda_L t}, \tag{2}$$

where λ_L is the (Lagrangian) maximum Lyapunov exponent [10]; a value $\lambda_L > 0$ means Lagrangian chaos. The chaotic regime holds as long as the trajectory separation remains sufficiently smaller than the characteristic scale δ_R. Under these conditions, relative dispersion is often referred to as a nonlocal process because it is mainly driven by the deformation field at scales much larger than the particle separation. When $\delta > \delta_R$, on the other hand, the presence of an inverse energy cascade with spectrum $E(k) \sim k^{-5/3}$ implies a rough velocity field; in this case one expects

$$\langle R^2(t)\rangle \sim t^3, \tag{3}$$

that is Richardson superdiffusion [11]. This dispersion regime is said to be local, because the growth of the distance between two particles is now controlled by local velocity differences, i.e. mean gradients on a finite scale of the order of the particle separation. In the limit of very large particle separations, namely larger than any scale of motion, the two trajectories are sufficiently distant from each other to be considered uncorrelated and the mean square relative displacement behaves like:

$$\langle R^2(t)\rangle \simeq 4K_E t, \quad \text{for } t \to \infty \tag{4}$$

where K_E is the asymptotic eddy-diffusion coefficient [11]. At any time t, the diffusivity $K(t)$ can be defined as:

$$K(t) = \frac{1}{4}\left\langle \frac{dR^2}{dt}(t)\right\rangle = \frac{1}{2}\left\langle R(t)\frac{dR}{dt}(t)\right\rangle \tag{5}$$

with $K(t) \to K_E$ for $t \to \infty$.

Relative dispersion is a fixed-time indicator. This involves averaging, at a given time, particle separations that can be very different, which can be problematic for multiscale turbulent flows, especially in a local dispersion regime.

Another approach, allowing to disentangle contributions to the dispersion process from different scales, is to resort to indicators that are, instead, computed as fixed-scale averages. The finite-scale Lyapunov exponent (FSLE) has been formerly introduced as the generalization of the maximum Lyapunov exponent (MLE) λ for non-infinitesimal perturbations [12]. If δ is the size of the perturbation on a trajectory in the phase space of a system, and $\langle \tau(\delta) \rangle$ is the phase space averaged time that δ takes to be amplified by a factor $\rho > 1$, then the FSLE is defined as

$$\lambda(\delta) = \frac{1}{\langle \tau(\delta) \rangle} \ln \rho. \tag{6}$$

The quantity $\tau(\delta)$ is the exit time of the perturbation size from the scale δ, and it is defined as the first arrival time to the scale $\rho \cdot \delta$, with $\rho \sim O(1)$. The evolution equations of Lagrangian trajectories form a dynamical system whose phase space is the physical space spanned by the trajectories. In this context, the analysis of relative dispersion can be treated as a problem of finite-size perturbation evolution, with scale-dependent growth rate measured by the FSLE. By a dimensional argument, if relative dispersion follows a $\langle R^2(t) \rangle \sim t^{2/\beta}$ scaling law, then the FSLE is expected to scale as $\lambda(\delta) \sim \delta^{-\beta}$. For example, in case of standard diffusion we expect $\beta = 2$; for Richardson superdiffusion, $\beta = 2/3$; in ballistic or shear dispersion we have $\beta = 1$. Chaotic advection means exponential separation between trajectories, which amounts to a scale-independent FSLE $\lambda(\delta) = $ constant, i.e. $\beta \to 0$. In the limit of infinitesimal separation, the FSLE is nothing but the MLE, i.e. $\lambda(\delta) \simeq \lambda_L$.

An indicator related to the FSLE is the mean square velocity difference between two trajectories as function of their separation. Indicating with $\mathbf{r}^{(1)}$, $\mathbf{r}^{(2)}$, $\mathbf{v}^{(1)}$, $\mathbf{v}^{(2)}$ the positions and the Lagrangian velocities of two particles 1 and 2 at a given time, we define the finite-scale relative velocity (FSRV) at scale δ,

$$\langle [\Delta V(\delta)]^2 \rangle = \langle \left[\mathbf{v}^{(1)} - \mathbf{v}^{(2)} \right]^2 \rangle \tag{7}$$

where the average is over all trajectory pairs fulfilling the condition $R(t) = ||\mathbf{r}^{(1)}(t) - \mathbf{r}^{(2)}(t)|| = \delta$ at some time t. From the FSRV a scale-dependent diffusivity can be formed as $K(\delta) = (1/2)\delta \langle [\Delta V(\delta)]^2 \rangle^{1/2}$ and compared to the classical time-dependent diffusivity $K(t)$ defined in (5).

3   Drifter data set

The data used in this study come from a set of 175 satellite-tracked ocean drifters deployed at Campos and Santos Basins - Southeastern Brazil - for environmental assessments of oil and gas activities (MONDO projects), and from Projeto AZUL [4], a pilot operational oceanography project for the region. The period of analysis ranges from September 2007 to September 2014. Deployments carried out during MONDO projects occurred from 2007 to 2012 (with the exception of 2008), while deployments from Projeto AZUL started in 2013. Part of the drifters were deployed in clusters of 3 to 5 units, with initial pair separations smaller than 1 km, in order to study dispersion properties (as

performed in [3]). Other deployments were targeted at dynamic features of the region like eddies and meanders and consisted in releasing either a single buoy at a time or groups with greater initial pair separations. All drifters are of SVP (Surface Velocity Program) type [13], with an underwater drogue attached to a surface buoy, an arrangement designed to minimize wind slippage and to represent the average current of the top 20-m layer of the ocean. Each drifter is equipped with a GPS device and iridium communication, allowing for a 7 m accuracy of the position and a fixed 3 h acquiring rate. Data were quality controlled as proposed by the Global Drifter Program [14] to remove spurious values and to assure that trajectories pertain to the period when the drifter was in the water and with the drogue attached. Resulting trajectory durations vary from 30 to 671 days, with a mean of 180 days and a standard deviation of 132 days. In order to remove high-frequency components, a Blackman low-pass filter of 25 h was applied to the data. Despite the heterogeneity of the deployment strategies and frequency, the 175 trajectories analyzed provide a rather good sampling of the southwestern corner of the South Atlantic gyre and suffice for two-particle statistics studies. Trajectories and deployment locations are presented in Fig. 1.

The domain explored by the drifters mainly corresponds to that of the southward flowing Brazil Current and to the area where this meets the northward flowing Malvinas Current, forming the Brazil-Malvinas Confluence, a highly energetic zone playing an important role in weather and climate of South America. More details about the local oceanography can be found in [3] and references therein. Here we only recall that this is an area of intense mesoscale activity with eddies detaching from both sides of the flow and that the first internal Rossby radius of deformation has a meridional variation in the range $(20 - 40)$ km, in the region.
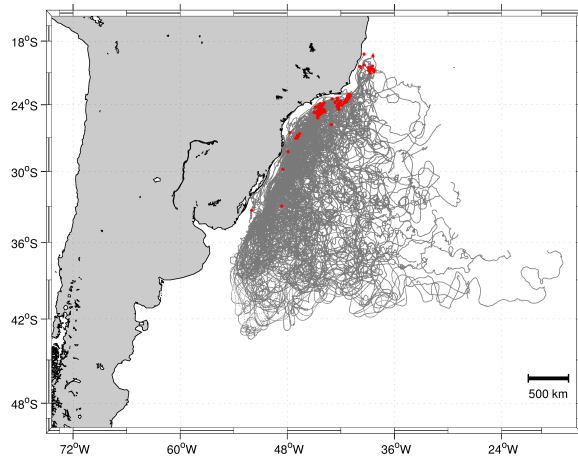

Fig. 1. Overall view of drifter trajectories. The larger red dots indicate the Lagrangian origins of trajectories.

4   Analysis of two-particle statistics

In this section we present the results of the data analysis on two-particle statistics. Distances between two points on the ocean surface are calculated as great circle arcs, according to the spherical geometry standard approximation. The available statistics is limited by finite lifetime of trajectories and irregular deployments of drifters in time. Hence, in order to increase the statistics, besides the original pairs we also consider chance pairs, that is pairs that happen to be sufficiently close to each other at an arbitrary instant of time after their release [15].

Relative dispersion is reported in the left panel of Fig. 2 for three different initial separations. The numbers of pairs counted in the statistics depends on the initial threshold: 64 for $R(0) \leq 2$ km, 77 for $R(0) \leq 5$ km and 91 for $R(0) \leq 10$ km. The dependence of $\langle R^2(t) \rangle$ on $R(0)$ is well evident. The early regime is shown in the right panel and it does not display any clear exponential growth of $\langle R^2(t) \rangle$. In the opposite limit of very large times, corresponding to separations $\delta \geq (250 - 300)$ km, some tendency towards a linear scaling, indicating diffusive behavior, is found. In the intermediate range between these two, the scaling of relative dispersion is not far from t^3, as for Richardson superdiffusion, but the growth is somehow smaller.
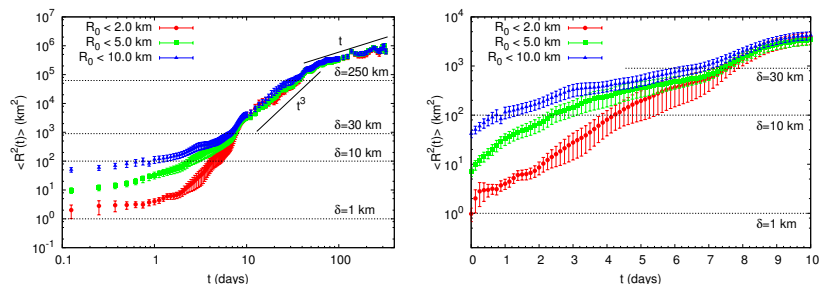

Fig. 2. Drifter relative dispersion $\langle R^2(t) \rangle$ (left panel) and its early regime (right panel) for initial separations as in the legend. The time sampling is $\Delta t = 1/8$ day. Error bars are the standard deviations.

Relative diffusivity in the zonal and meridional directions, for $R(0) \leq 2$ km, is plotted in Fig. 3. In the intermediate time range between 10 and 100 days the behavior of $K(t)$ approaches a t^2 law, as expected in the Richardson dispersion regime. The diffusivity in the meridional direction is found to be larger, reflecting the anisotropy of the flow.

We now present the results obtained with fixed-scale indicators. These have been evaluated for the same initial thresholds, $R(0) \leq 2, 5, 10$ km. The density of scales is fixed by setting $\rho = 1.3$ or $\rho = \sqrt{2}$, representing a good compromise between the finest possible scale resolution and the largest possible number of pairs per threshold to ensure convergence of the statistics. The results do not strongly depend on the precise value of the amplification factor. The maximum
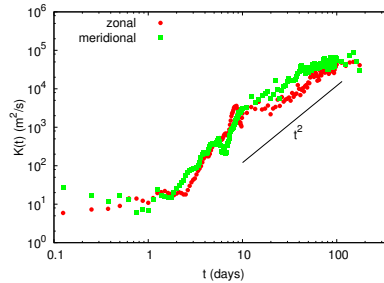
Fig. 3. Drifter relative diffusivity $K(t)$ for zonal and meridional components, for initial separations $R(0) \leq 2$ km. The t^2 scaling corresponds to the Richardson regime. The time sampling is $\Delta t = 1/8$ day.

number of pairs considered varies with the initial threshold: 64 for $R(0) \leq 2$ km, 77 for $R(0) \leq 5$ km, 90 for $R(0) \leq 10$ km.

The FSLE is plotted in Fig. 4; the comparison of left and right panels ($\rho = 1.3$ and $\rho = \sqrt{2}$, respectively) clearly shows the robustness of results with respect to the value of ρ. In the mesoscale range $\delta > \delta_R$ above the deformation radius, here reasonably estimated as $\delta_R \simeq 30$ km, the FSLE exhibits a power law scaling $\delta^{-2/3}$ compatible with Richardson superdiffusion and local dispersion. At scales of the order of the deformation radius $\delta \approx \delta_R$, the FSLE is close to a constant value $\lambda(\delta) \simeq 0.15$ day^{-1}, suggesting exponential separation and a less local dispersion process. These results are in good agreement with those previously found, in the same scale ranges, using data from the first MONDO project [3]. In principle, they could support a classical double-cascade scenario with $k^{-5/3}$ and k^{-3} kinetic energy spectra in the inverse energy cascade and in the direct enstrophy cascade, respectively. However, in the submesoscale range $\delta \simeq (1-10)$ km well below δ_R we find a behavior close to $\lambda(\delta) \sim \delta^{-1/2}$, implying enhanced scale-dependent dispersion rates. We observe, furthermore, that such a power-law scaling of the FSLE would correspond to a rather flat kinetic energy spectrum in k^{-2}. At the smallest sampled scales ($\delta < 1$ km) the FSLE tends to level off, which is more clearly seen for $\rho = 1.3$ (left panel of Fig. 4). However, we remark that on these scales the resulting values are likely affected by poorer statistics and filtering issues (the time scale $1/\lambda(\delta) \approx 1$ day is of the order of the filtering time window of 25 h).

The computation of the mean square finite size relative velocity is reported in Fig. 5 (left panel). The Lagrangian velocity components are obtained from the drifter trajectories by a standard finite differencing method. The FSRV is consistent with Richardson dispersion for scales larger than the Rossby radius, where it scales as $\delta^{2/3}$. In a rather narrow intermediate range ($\delta \approx \delta_R$) it gets closer to a δ^2 behavior, suggesting exponential separation. In the submesoscale range $(1-10)$ km, on the other hand, it appears to scale as δ, which is consistent with a k^{-2} kinetic energy spectrum and the FSLE behavior found in the same scale range. These results support a classical double-cascade phenomenology only at scales comparable to the Rossby radius or larger, while they suggest more energetic submesoscales well below δ_R. From the FSRV an "equivalent
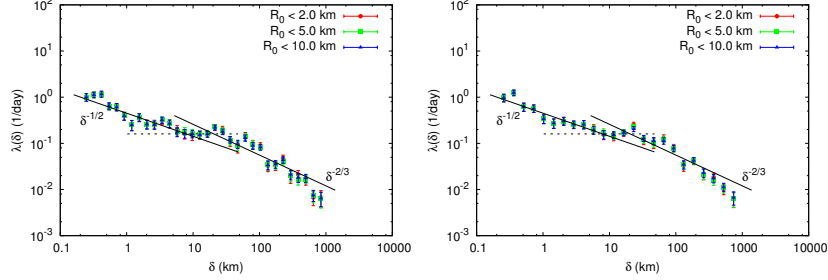
Fig. 4. FSLE for different values of $R(0)$, as in the legend, and amplification factor $\rho = 1.3$ (left panel) and $\rho = \sqrt{2}$ (right panel). The $\delta^{-2/3}$ and $\delta^{-1/2}$ scalings respectively correspond to Richardson law and a k^{-2} spectrum. The horizontal dashed line corresponds to $\lambda(\delta) \simeq 0.15\,\mathrm{day}^{-1}$. Error bars are the standard deviations of the mean values.

Lagrangian spectrum" $E_L(k) = \langle [\Delta V(k)]^2 \rangle / k$ can be dimensionally defined replacing δ with $2\pi/k$. This quantity returns the same picture, in k space, as that found with the FSRV (Fig. 5, right panel).
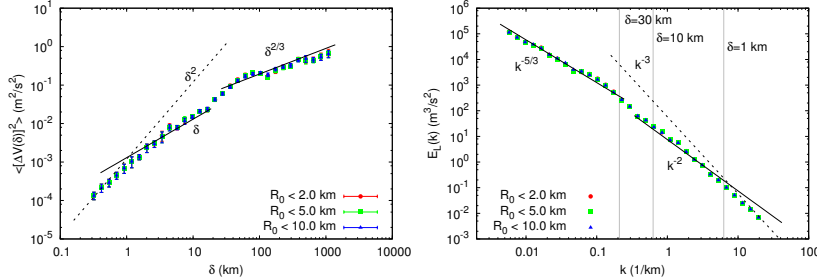

Fig. 5. Left: FSRV computed together with the FSLE. The scalings δ^2, δ and $\delta^{2/3}$ correspond to k^{-3}, k^{-2} and $k^{-5/3}$ energy spectra, respectively. Error bars are the standard deviations of the mean values; here $\rho = 1.3$. Right: Equivalent Lagrangian spectrum defined from the FSRV. The Rossby radius $\delta_R \simeq 30$ km corresponds to wavenumber $k \simeq 0.2$.

Finally, in Figure 6 we compare the diffusivity computed as a fixed-time average, Eq. (5), with that computed as a fixed-scale average from the FSRV. Both quantities are plotted as function of the separation between two drifters: $K(\delta) = (1/2)\delta \langle [\Delta V(\delta)] \rangle^{1/2}$ with δ as the independent variable, and $K(t)$ versus $\delta = \langle R^2(t) \rangle^{1/2}$ where the independent variable is the time t. The $\delta^{4/3}$ regime in the mesoscales range and the δ^2 one in the narrow intermediate range $\delta \approx \delta_R$ (here less evident than with other indicators) are respectively consistent with Richardson superdiffusion and nonlocal dispersion. Hence, they may support the presence of an inverse cascade with $E(k) \sim k^{-5/3}$ (at scales $\delta > \delta_R$) and a direct cascade with $E(k) \sim k^{-3}$ (at scales $\delta \approx \delta_R$), as predicted by QG turbulence theory. Nevertheless, the $\delta^{3/2}$ scaling, corresponding to a k^{-2} spectrum, found for $\delta \simeq (1-10)$ km confirms that dispersion is local in this
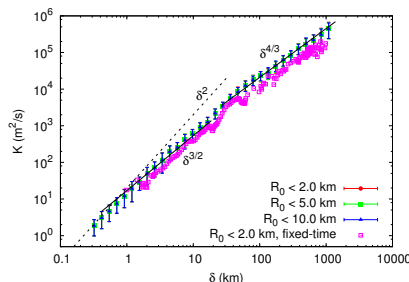
Fig. 6. Diffusivity as a function of the separation: fixed-time average $K(t)$ vs $\delta = \langle R^2(t)\rangle^{1/2}$ and fixed-scale average $K(\delta)$ vs δ. The $\delta^{4/3}$, $\delta^{3/2}$ and δ^2 correspond to $k^{-5/3}$, k^{-2} and k^{-3} spectra, respectively.

scale range and that submesoscales are more energetic than expected in a direct enstrophy cascade.

5   Numerical results

We now compare the results of the drifter data analysis with those issued from numerical simulations of the Lagrangian dispersion process in the same geographical area in the period 20/9/2007-21/10/2008 (corresponding to MONDO project). More details about the numerics can be found in [3]. Here we simply recall that $O(10^2)$ virtual trajectories are considered and that the spatial resolution of the model (HYCOM, see e.g. [16]) generating the advecting surface flow is approximately 7 km.

Two numerical experiments, that we indicate with E1 and E2, were conducted. In the first one (E1) the drifters are uniformly deployed in an area of about (10×10) km^2 centered around a position corresponding to the mean initial location of MONDO drifters. The average initial distance between synthetic particle pairs is $\langle R(0)\rangle \simeq 5$ km. The lifetime of trajectories is between 150 days and 200 days. In the second experiment (E2) the initial distribution of the drifters is characterized by larger separations, namely comparable to the spacing of the numerical grid (~ 10 km); the average initial distance between particle pairs is $\langle R(0)\rangle \simeq 40$ km and the duration of trajectories is $(250 - 400)$ days.

For the comparison between the results obtained from real and model trajectories, here we focus on the FSLE and the FSRV, Fig. 7, but a similar picture is returned by other indicators too. To increase the statistics we now select trajectories with a larger initial separation: $R(0) < 50$ km (similar results are found for smaller values of $R(0)$, though they are more noisy). Moreover we set the amplification factor to $\rho = \sqrt{2}$. The behaviors of both FSLE and FSRV support a double-cascade scenario on scales comparable to those found with actual drifters. The plateau value of FSLE at scales $O(\delta_R)$ is very close to the one found in the real experiments, $\lambda(\delta) \simeq 0.15$ day^{-1}. At larger scales, for both numerical experiments E1 and E2 the behavior of FSLE is compatible with $\lambda(\delta) \sim \delta^{-2/3}$, supporting Richardson dispersion and an inverse energy

cascade process. Experiment E2, which is characterized by longer trajectories, shows a clearer scaling, thanks to a larger number of pairs reaching this range of large scales. Mean square velocity differences in the same range of scales display a reasonably clear $\delta^{2/3}$ scaling, also supporting an inverse energy cascade, with values close to those found with actual drifters. At separations smaller than the Rossby deformation radius, both indicators point to the presence of a direct enstrophy cascade: the FSLE is constant and the FSRV behaves as $\langle[\Delta V(\delta)]^2\rangle \sim \delta^2$. This only partially agrees with the results found for real drifters, namely only in the scale range $10\ \mathrm{km} < \delta < 30\ \mathrm{km}$. At subgrid scales, velocity field features are not resolved and relative dispersion is necessarily a nonlocal exponential process driven by structures of size of the order of (at least) the Rossby radius. Correspondingly, the FSLE computed on model trajectories does not display the enhanced dispersion regime (with $\lambda(\delta) \sim \delta^{-1/2}$) at scales smaller than 10 km.
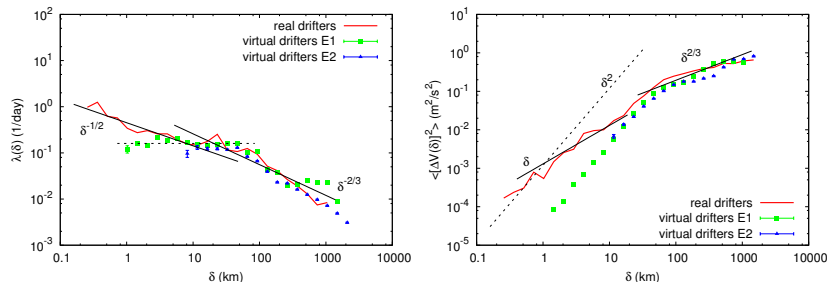

Fig. 7. FSLE (left panel) and FSRV (right panel) for $R(0) \leq 50$ km and $\rho = \sqrt{2}$ for real and virtual drifters from numerical experiments E1 and E2. For virtual drifters errors are on the order of point size. The large-scale saturation of the FSLE (E1) depends on the value of the trajectory integration time.

6   Conclusions

In this study we considered a set of surface drifter trajectories to analyse relative dispersion in the Southwestern Atlantic Ocean, by means of both fixed-time and fixed-scale statistical indicators. Fixed-time indicators, like the mean square displacement and the relative diffusivities as functions of the time lag from the release, point to a long-time regime compatible with Richardson superdiffusion, at least to some extent. As for the early regime of dispersion, no clear evidence of exponential separation is detected.

Scale-dependent indicators (FSLE, FSRV and related quantities) seem to more clearly reveal the different dispersion regimes, compatibly with the available statistics and the nonhomogeneous and nonstationary characteristics of the flow. In the mesoscale range $\delta \approx (30 - 300)$ km, both the FSLE and the FRSV display scaling behaviors compatible with Richardson superdiffusion and a 2D inverse energy cascade scenario. In a rather narrow range of scales close

to the Rossby radius of deformation $\delta_R \simeq 30$ km, a more nonlocal dispersion regime is found, indicative of exponential separation and, possibly, compatible with a 2D direct enstrophy cascade. However, at scales considerably smaller than δ_R, particularly for $\delta \approx (1-10)$ km, enhanced relative dispersion is observed, corresponding to the scaling $\lambda(\delta) \sim \delta^{-1/2}$ of the FSLE. Such a local dispersion regime suggests energetic submesoscale motions compatible with a kinetic energy spectrum $E(k) \sim k^{-2}$, as found in high-resolution numerical simulations of upper-layer ocean turbulence [8,9]. It is interesting to observe that evidences of increased dispersion rates and energetic submesoscales have been recently reported also in other studies based on Lagrangian drifter data, in different regions of the world oceans [17–19].

The data analysis was compared with the results of numerical simulations of the Lagrangian dynamics performed with a general circulation model. The comparison shows that the characteristics of the relative dispersion process found with real drifters are consistent with those obtained with virtual ones for scales $\delta \gtrsim \delta_R \simeq 30$ km. The model, however, fails to reproduce a local dispersion regime in the submesoscale range $(1-10)$ km, of course due to its finite spatial resolution (which is of the order of 10 km) and does not allow to address the dynamical role played by very small scale flow features.

We would like to conclude mentioning that further investigation on submesoscale processes would be extremely useful to clarify the origin of the observed deviations from classical QG turbulence. In particular, we believe that taking into account seasonality effects could allow to get more insight on relative dispersion at submesoscales in the region. This is left for future work.

References

1. H.A. Figueroa, D.B. Olson. Lagrangian statistics in the South Atlantic as derived from SOS and FGGE drifters. J. Mar. Res. **47**, 525–546 (1989).
2. H. Schäfer, W. Krauss. Eddy statistics in the South Atlantic as derived from drifters drogued at 100 m. J. Mar. Res. **53**, 403–431 (1995).
3. S. Berti, F. dos Santos, G. Lacorata, A. Vulpiani. Lagrangian drifter dispersion in the southwestern Atlantic Ocean. J. Phys. Oceanogr. **41**, 1659–1672 (2011).
4. F. dos Santos et al. Projeto Azul: operational oceanography in an active oil and gas area southeastern Brazil in *Coastal Ocean Observing System*, Elsevier (2015).
5. R.H. Kraichnan. Inertial ranges in two-dimensional turbulence. Phys. Fluids **10**, 1417–1423 (1967).
6. J.G. Charney. Geostrophic turbulence. J. Atmos. Sci. **28**, 1087–1094 (1971).
7. J.C. McWilliams. Submesoscale, coherent vortices in the ocean. Rev. Geophys. **23**, 165–182 (1985).
8. X. Capet, J.C. McWilliams, M.J. Molemaker, A.F. Shchepetkin. Mesoscale to submesoscale transition in the California current system. Part I: flow structure, eddy flux, and observational tests. J. Phys. Oceanogr. **38**, 29–43 (2008).
9. P. Klein, B.L. Hua, G. Lapeyre, X. Capet, S. Le Gentil, H. Sasaki. Upper ocean turbulence from high-resolution 3D simulations. J. Phys. Oceanogr. 38, 1748–1763 (2008).
10. G. Boffetta, A. Celani, M. Cencini, G. Lacorata, A. Vulpiani. Non-asymptotic properties of transport and mixing. Chaos **10**, 50–60 (2000).

11. L.F. Richardson. Atmospheric diffusion shown on a distance-neighbor graph. Proceedings of the Royal Society A **100**, 709–737 (1926).
12. E. Aurell, G. Boffetta, A. Crisanti, G. Paladin, A. Vulpiani. Growth of non-infinitesimal perturbations in turbulence. Phys. Rev. Lett. **77**, 1262–1265 (1996).
13. A.L. Sybrandy, P.P. Niiler. WOCE/TOGA SVP Lagrangian drifter construction manual. Scripps Institution of Oceanography Rep. 91/6, 58 pp. (1991).
14. D.V. Hansen, P.M. Poulain. Quality control and interpolations of WOCE-TOGA drifter data. J. Atmos. Oceanic Technol. **13**, 900–909 (1996).
15. J.H. LaCasce. Statistics from Lagrangian observations. Prog. Oceanogr. **77**, 1–29 (2008).
16. R. Bleck, S. Benjamin. Regional weather prediction with a model combining terrain-following and isentropic coordinates. Part I: model description. Mon. Wea. Rev. **121**, 1770–1785 (1993).
17. R. Lumpkin, S. Elipot. Surface drifter pair spreading in the North Atlantic. J. Geophys. Res. **115**, C12017, 1–20 (2010).
18. K. Schroeder, J. Chiggiato, A.C. Haza, A. Griffa, T.M. Özgökmen, P. Zanasca, A. Molcard, M. Borghini, P.M. Poulain, R. Gerin, E. Zambianchi, P. Falco, C. Trees. Targeted Lagrangian sampling of submesoscale dispersion at a coastal frontal zone. Geophys. Res. Lett. **39**, 11608, (2012).
19. A.C. Poje et al. Submesoscale dispersion in the vicinity of the Deepwater Horizon spill. Proc. Natl. Acad. Sci. U.S.A., 111, 12693-12698 (2014).